Constraining the Flow and Thickness History of Siple Dome, West Antarctica

S.F. Price, H. Conway, and E.D. Waddington

Department of Earth and Space Sciences, University of Washington, Seattle Washington, 98195

1. Introduction and Study Motivation

From 1997-1999 a ~1000 m long ice core was recovered from Siple Dome, West Antarctica (Fig. 1). Coincident with core recovery were numerous glaciological and geophysical studies that recorded the dome geometry, ice surface velocities, internal stratigraphy from ice penetrating radar, and ice temperature. More recently, a depth-age profile for the core has been published (Taylor and others, 2005) and new estimates for the accumulation rate history have become available (M. Spencer and R. Alley, Penn State Univ., personal comm.).

We use these data and a thermomechanical, flowband model to constrain the flow and thickness history at Siple Dome. We assume that the accumulation rate and surface temperature histories are known and vary a number of poorly constrained model inputs (the timing of divide-flow onset, the thickness history, flow enhancement, and accumulation rate scouring) in order to match model ouput to observations. In doing so, we place constraints on the unknown model inputs.

The model solves the full, 2-dimensional heat and stress-balance equations using the Finite Volume Method. A brief introduction to the method is given in section 2. In section 3 we validate model output by comparing it with well known analytical solutions and the results from previous work. Application of the model to Siple Dome is described in section 4. In sections 5 and 6 we present favored values for the model inputs along with a sensitivity analysis. Discussion and conclusions are given in Section 7.

Figure 1: Study Area

2. Solution to Governing Equations: The Finite Volume Method

The Finite Volume Method (FVM; Patankar, 1980) shares similarities with both finite-difference and finite-element methods (FDMs and FEMs). Like FDMs, the FVM use a structured grid. Centered differences are used to approximate 1st order derivatives to 2nd order accuracy. Like FEMs, FVMs solve the integral form of the governing differential equations at each respective "element" (here referred to as "volumes"). Consider the volume (grey area) centered at point P in Figure 2a, with neighboring volumes to the East, West, Up and Down (E, W, U, D) and interfaces between volumes at points e, w, u and d. The advective-diffusive differential equation governing the conservation of some scalar quantity ϕ, with diffusivity Γ, and source term S is

$$\frac{\partial(\rho\phi)}{\partial t}+u_i\frac{\partial(\rho\phi)}{\partial x_i}=\frac{\partial}{\partial x_i}\left(\Gamma\frac{\partial\phi}{\partial x_i}\right)+S, \qquad (i=x,z)$$

To simplify the example of discretization with FVMs, consider the case of steady state with no advection,

$$\frac{\partial}{\partial x}\left(\Gamma\frac{\partial\phi}{\partial x}\right)+\frac{\partial}{\partial z}\left(\Gamma\frac{\partial\phi}{\partial z}\right)+S=0.$$

Integration over the finite volume centered at P in Figure 2a gives

$$\int_d^u\int_w^e\frac{\partial}{\partial x}\left(\Gamma\frac{\partial\phi}{\partial x}\right)dxdz+\int_w^e\int_d^u\frac{\partial}{\partial z}\left(\Gamma\frac{\partial\phi}{\partial z}\right)dzdx+\int_u^d\int_w^e S dzdx=0,$$

$$\Gamma_e\left.\frac{\partial\phi}{\partial x}\right|_e\Delta z-\Gamma_w\left.\frac{\partial\phi}{\partial x}\right|_w\Delta z+\Gamma_u\left.\frac{\partial\phi}{\partial z}\right|_u\Delta x-\Gamma_d\left.\frac{\partial\phi}{\partial z}\right|_d\Delta x+\bar{S}\Delta x\Delta z=0.$$

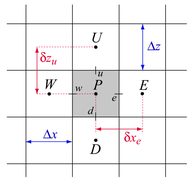

Figure 2a: Finite volume centered at point P, with neighbors E, W, U, D and interfaces e, w, u, and d.

If the coordinate direction across interface e (i.e. from volume P to volume E) is orthogonal to the interface e, then the flux across that face is due entirely to the gradient in ϕ between points P and E. This is an important requirement for FVMs. A similar constraint for flux across the other interfaces gives

$$\Gamma_e\left(\frac{\phi_E-\phi_P}{\delta x_e}\right)\Delta z-\Gamma_w\left(\frac{\phi_P-\phi_W}{\delta x_w}\right)\Delta z+\Gamma_u\left(\frac{\phi_U-\phi_P}{\delta z_u}\right)\Delta x-\Gamma_u\left(\frac{\phi_U-\phi_P}{\delta z_u}\right)\Delta x+\bar{S}\Delta x\Delta z=0.$$

Note that uniform values for the diffusivity and grid spacing are not required. Next, we define coefficients

$$a_W=\frac{\Gamma_w\Delta z}{\delta x_w}, \quad a_U=\frac{\Gamma_u\Delta x}{\delta z_u}, \quad a_D=\frac{\Gamma_d\Delta x}{\delta z_d}, \quad a_E=\frac{\Gamma_e\Delta z}{\delta x_e}, \quad a_P=a_E+a_W+a_U+a_D.$$

With b defined as the integrated source term and, after including the boundary conditions, we obtain the following set of n linear equations in n unknowns,

$$a_P\phi_P=a_E\phi_E+a_W\phi_W+a_U\phi_U+a_D\phi_D+b=\sum_1^n a_n\phi_n+b\ ,$$

which can be rearranged to

$$\mathbf{A}\vec{\phi}=\vec{b}\ .$$

A is a banded sparse matrix of coefficients, $\vec{\phi}$ is the vector of unknowns and $\vec{b}$ is the vector of source terms. The grid and profile assumptions result in a sparse matrix structure with only 5 non-zero diagonals (Figure 2b).

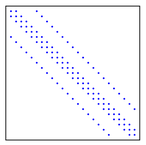

Figure 2b: Non-zero elements of coefficient matrix **A** for a 5x5 domain of finite volumes.

3. Model Validation

We validate the model by comparing numerical solutions to well known analytical solutions that use simplified domain geometries and boundary conditions. For more complicated domain geometries and boundary conditions, qualitative comparisons are made.

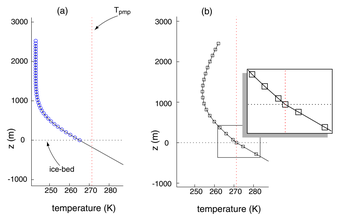

Figure 3a: (a) Steady-state temperatures at a flow divide for an arbitrary, parabolic shaped ice sheet with constant T_{surf} of -243 K and $\dot{b}$ of 0.33 m a^{-1}. To allow comparison between the analytical* (blue circles) and model (black line) solutions, u was set to 0, w was specified as linear from -$\dot{b}$ at the surface to 0 at the bed and thermal properties were held constant. The mean and maximum differences are 0.004 K and 0.037 K, respectively.

* Paterson (1994), pp. 216-220

(b) Temperature solution demonstrating the effects of horizontal advection, for a surface temperature that warms in the downstream direction and non-zero u. Basal melting is also evident, as indicated by the "kink" in the basal temperature gradient.

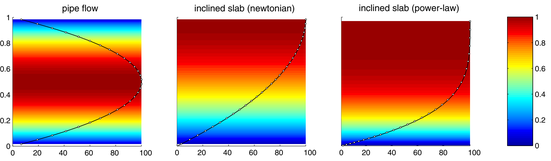

Figure 3b: Non-dimensional solutions to the momentum equations for boundary conditions consistent with pipe flow (left), Newtonian-viscous flow (middle) and power-law (n=3) viscous-flow (right) down an inclined plane. Colormaps show the normalized, horizontal velocity for a 1x100 domain on a 20x30 grid. Overlain are analytical (solid) and model (dots) shape functions. Vertical velocity fields, which should all be ~0, are O~10^{-8}-10^{-14} relative to u_{max}=1*)*.

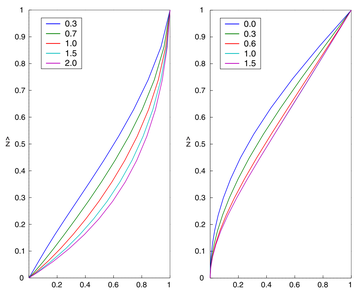

Figure 3c: A non-trivial test of the momentum balance model is made by comparing the normalized horizontal (left) and vertical (right) velocity profiles near to, and far from, an ice divide. Colored lines identify profiles within n units of ice thickness from the divide. Away from the divide, $u(z)$ becomes more parabolic and $w(z)$ becomes more linear. Far from the divide $u(z)$ and $w(z)$ approach profile shapes given by laminar flow (i.e. become more similar to the magenta colored lines). These results are comparable to those given by Raymond (1983).

The relatively slower vertical velocity at a given depth nearer to the divide, relative to the same depth on the flank, result in the upwarped isochrons (see Figure 4b) and isotherms observed at ice divides.

5. Application to Siple Dome

Surface accumulation rate and temperature histories force changes to the model velocity and temperature fields over the last 120 ka. While both histories are preliminary and likely to change somewhat, we take them as absolutes here. The geothermal flux is held constant at 0.072 W m^{-2}. Velocity boundary conditions are specified so that the surface-accumulation rate integrated from the divide to a domain boundary is balanced by the flux across that boundary; surface geometry can change over time but the domain volume is held constant. To force thinning or thickening of the dome, we increase or decrease flux at the margins, relative to the balance flux. Similarly, assymetrical flux changes are used to force migration of the ice divide.

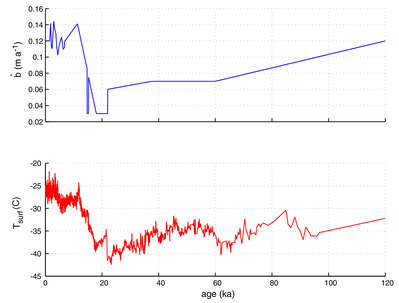

Figure 4a: Accumulation rate (top) and surface temperature (bottom) histories used to force the model over the last 120 ka. Accumulation rates from ~25 ka BP onward are based on bubble counts and firn modeling (M. Spencer and R. Alley (PSU)). Surface temperatures are preliminary estimates based on analysis of stable isoptopes from the Siple Dome ice core (courtesy of J. White and A. Schilla (UC)).

Figure 4B: Model output includes 2d temperature and veocity fields, a 2d array of internal layer shapes (below), and domain shape. These output fields are compared to observations from Siple Dome including the measured depth-temperature profile, the observed depth vs. divide-bump amplitude, the depth-age profile, and the dome surface shape.

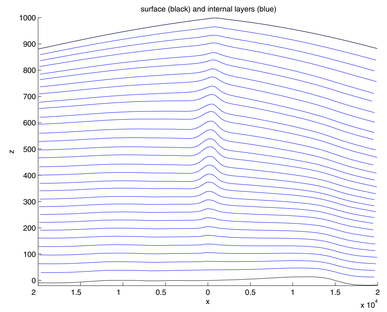

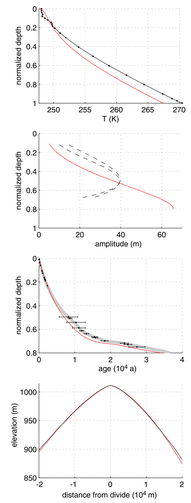

Figure 4C (left): Model (red line) fit to observations (black) from Siple Dome. In this reference case, changes are forced solely by the accumulation and temperature histories in Figure 4a, there is no change in dome thickness, and a divide is considered to be in place for the entire model run. Top: temperature-depth profile (observed temperature profile is from Engelhardt (2004)). 2nd from top: divide-bump amplitude profile (observed amplitudes from RES of Jacobel and others (2000)). 2nd from bottom: age-depth profile (observed profile from Taylor and others (2005)). Bottom: dome surface profile. In general, the model fit is acceptable for only the dome surface profile.

Figure 4D (right): As discussed by Pettit (2003), ice in the lower ~300 m of Siple Dome is both recrystallized (from 0-200m off the bed) and exhibits a c-axis-oriented fabric (from 200-300m off the bed).

To simulate "stiff", re-crystallized ice near the bed, we use a scalar enhancement factor, E<1. To simulate the effects of the the c-axis-oriented layer using a scalar enhancement factor, a special procedure is required. We use a modified version of Wang and Warner's (1998) method for calculating a spatially variable E based on the shear and compressive fractions of the total strain rate: where compression dominates (near the divide) E<1, where horizontal-shear dominates (on the flanks) E>1. In between, E varies smoothly.

To "tune" our enhancement factor, we choose values for $E_{compressive}$ and E_{shear} so that our vertical-velocity shape functions approximate those of Pettit (2003) (upper panel). The "false bed" effect discussed by Pettit (2003) can be seen in horizontal velocity shape functions (middle panel), where the majority of the deformation takes place above ~200m off the bed. A contour plot of our favored enhancement factor is show to the right.

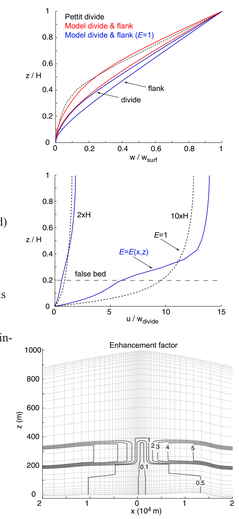

5. Fitting the Observations

To the right (5a), we show the best model fit (red) to the observed (black) temperature, bump amplitude, and age-depth profiles, and to the observed surface shape. The model fit corresponds to:

- thinning of 350m from 16-2ka BP
- onset of divide flow at 3ka BP.
- divide scouring at 3% of the modern $\dot{b}$
- enhancement, E=E(x,z), starting at 7 ka BP

Also shown to the right (b) is the model-observation misfit (modeled - observed value). Using these misfit values as a reference, we explore the sensitivity of the model-observation misfit when we perturb the model from the favored values noted above.

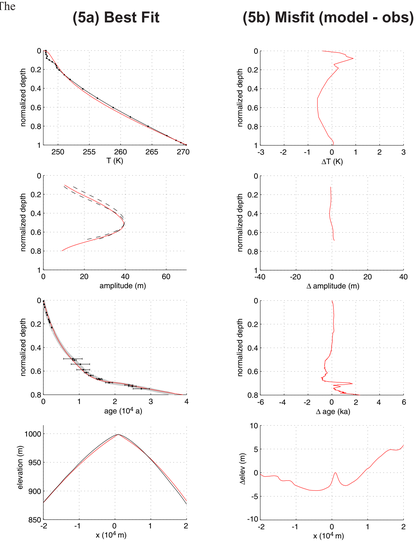

6. Sensitivity (In all cases, the nominal misfit from Figure 5a is shown by the red, solid line)

(a) thickness change
250m of thinning (dash)
350m of thinning (solid)
450m of thinning (dot)

(b) divide-onset time
2ka BP (dash)
3ka BP (solid)
5ka BP (dot)

(c) divide scouring
1.5% of modern accum. rate (dash)
3% of modern accum. rate (solid)
6% of modern accum. rate (dot)

(d) flow enhancement
Red: E(x,z) at 4(dash), 7(solid), 10(dot) ka BP
Blue: E(x,z) averaged horizontally
Black: E=1

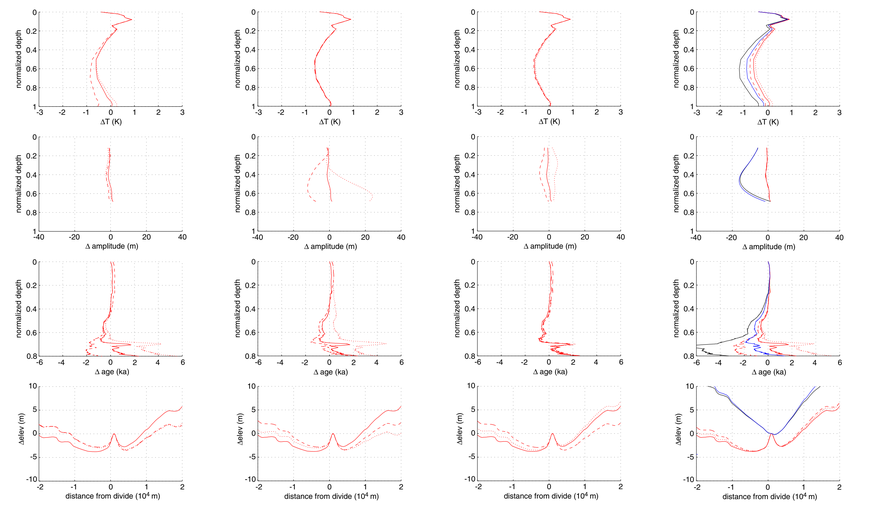

7. Discussion and Conclusions

By fitting model output to observations at Siple Dome, we conclude that:

- Siple Dome thinned by 350m from 16-2 ka BP (within the range given by Waddington and others, 2005)
- Divide flow was initiated at 3 ka BP (followed by northward migration)
- Scouring at 3% of the modern accumulation rate has occured since 3 ka BP
- Spatially variable, flow enhancement (Fig.4d) has occured since 7 ka BP

For E=1, we have found no combination of model inputs that allows us to fit the observed bump-amplitude profile; for E=1, the bump amplitude is always too small and its maximum too deep. The "false bed" effect discussed by Pettit (2003) helps to explain this observation. We attempt to correct for the effects of various crystallographic-flow properties by applying a spatially variable E.

Like the bump-amplitude profile, the temperature-depth profile is difficult to reproduce; model temperatures at mid-depths are consistently too cold. Here, the fit to the temperature profile helps to constrain both upper and lower bounds to the total thickness change of the dome. For total thinning of <350 m, the temperature profile is too cool and for total thinning of >350 m the fit to the temperature *gradient* is increasingly worse (due to the effects of increased advective cooling). Our final "best fit" to the temperature profile is still as much as 0.5 K too cool. We find that glacial temperatures ~2 K warmer than those shown in Fig.4a improve upon this misfit. Possibly, our preliminary surface temperature history is too cool during the glacial.

The sensitivity analysis indicates that perturbations of ~100 m in thickness and ~2 ka in divide-flow onset time have a similar affect on the depth-age profile (the modern surface shape is largely unaffected). These effects may be further seperated from one another by examining the model fit to the observed depth-temperature and bump-amplitude profiles; the former is more sensitive to thickness changes and the latter is more senstive to divide-flow onset time.

The fits to all observations, other than the bump-amplitude profile, are insensitive to divide scouring. However, the bump-amplitude profile is sensitive to scouring rates that may be within the range of uncertainty of most accumulation-rate measurements (~5%). The affects of scouring and divide-flow onset time on the bump-amplitude profile are seperable because they affect the profile in a different manner (2nd panels in Figs. 6b and 6c) and, presumably, scouring occurs only after a divide is in place.

The fits to all observations are sensitive to flow enhancement. Here, only the temperature and depth-age profiles are sensitive to the length of time enhancement has been active for; several thousand years more or less of enhancement have an affect similar to ~100 m more or less of total thinning. Spatial variation in enhancement is necessary to fit the observed bump-amplitude profile. Removing that variation through, for example, horizonal averaging destroys not only the fit to the bump-amplitude profile, but to many of the other observations as well. The fit to the modern surface shape provides one obvious constraint on the available choices for enhancement. Figure 6d demonstrates that spatial averaging of the favored enhancement results in ice that is too soft, and a calculated dome shape that is too shallow.

References

Engelhardt, H. 2004. Ice temperature and high geothermal flux at Siple Dome, West Antarctica, from borehole measurements. *J. Glaciol.*, **50**(169), 251-256.

Jacobel R. W., Scambos, T. A., Nereson, N. A., and Raymond, C. F. 2000. Changes in the margin of Ice Stream C, Antarctica. *J. Glaciol.* **46**(152), 102-110.

Nereson, N.A., C.F. Raymond, E.D. Waddington and R.W. Jacobel. 1998. Recent migration of Siple Dome ice divide, West Antarctica. *J. Glaciol.*, **44**(148), 643-652.

Patankar, S.V. 1980. *Numerical Heat Transfer and Fluid Flow*. Hemisphere Publishing Corp., New York.

Paterson, W.S.B. 1994. *The Physics of Glaciers*. Oxford, Elsevier Publishing Ltd., 216-220.

Pettit, E. 2003. Unique dynamic behaviors of ice divides: Siple Dome and the rheological properties of ice. PhD disseration, *Univ. of Washington*.

Raymond, C.F. 1983. Deformation in the vicinity of divides. *J. Glac.*, **34**(117), 357-373.

Taylor, K., R.B. Alley, D.A. Meese, M.K. Spencer, E.J. Brook, N.W. Dunbar, R. Finkle, A.J. Gow, A.V. Kurbatov, G.W. Lamorey, P.A. Mayewski, E.J. Meyerson, K. Nishizumi, and G.A. Zielinski. 2005. Dating the Siple Dome (Antarctica) ice core by manual and computer interpretation of annual layering. *J. Glaciol.*, **50**(170), 453-461.

Waddington, E.D., H. Conway, E.J. Steig, R.B. Alley, E.J. Brook, K.C. Taylor, and J.W.C. White. 2005. Decoding the dipstick: Thickness of Siple Dome, West Antarctica, at the Last Glacial Maximum. *Geology*, **33**(4), 281-284.

Wang, W. L. and R. C. Warner (1998). Simulation of the influence of ice rheology on velocity profiles and ice-sheet mass balance. *Ann. Glaciol.*, 27, 194-200.